AIP | Review of Scientific Instruments

High definition imaging in the Mega Amp Spherical Torus spherical tokamak from soft x rays to infrared (invited)

P. G. Carolan, A. Patel, N. J. Conway, R. J. Akers, C. A. Bunting, et al.

Citation: Rev. Sci. Instrum. **75**, 4069 (2004); doi: 10.1063/1.1789583
View online: http://dx.doi.org/10.1063/1.1789583
View Table of Contents: http://rsi.aip.org/resource/1/RSINAK/v75/i10
Published by the American Institute of Physics.

High definition imaging in the Mega Amp Spherical Torus spherical tokamak from soft x rays to infrared (invited)

P. G. Carolan,[a] A. Patel, N. J. Conway, R. J. Akers, C. A. Bunting, G. F. Counsell, J. Dowling, M. R. Dunstan, A. Kirk, F. Lott, M. N. Price, and M. R. Tournianski
EURATOM/UKAEA Fusion Association, Culham Science Centre, Abingdon, Oxfordshire OX14 3DB, United Kingdom

M. J. Walsh
Walsh Scientific Ltd, Culham Science Centre, Abingdon, Oxfordshire OX14 3EB, United Kingdom

(The MAST Team)
EURATOM/UKAEA Fusion Association, Culham Science Centre, Abingdon, Oxfordshire OX14 3DB, United Kingdom

(Presented on 21 April 2004; published 12 October 2004)

The Mega Amp Spherical Torus (MAST) diagnostic needs are strongly influenced by physics goals that often require diagnostic integration and cross-mapping, especially in fine-scale investigations, such as transport barriers. Conversely, the unrivalled viewing access to the edge, scrape-off layer (SOL) and divertor regions, provided by the MAST open geometry, impacts on the physics program priorities. A supporting suite diagnostics, such as the high definition Thomson scattering systems, provide considerable added value in detailed data interpretation (e.g., bremsstrahlung emissivity in terms of Z_{eff}). Thus, to exploit these advantages, an extensive set of high-resolution imaging diagnostics have been installed, encompassing soft x-rays, visible bremsstrahlung, charge exchange recognisation radiation, D_α from NBI, and edge plasma neutrals, and infrared (IR) from the divertor and wall regions. Plasma light collection optics provide near parallel illumination of narrow bandpass interference filters to give monochromatic images. One adaptation provides multiwavelength images; another accommodates smooth variation of wavelength across an image (e.g., for a range of Doppler shifts beam fast neutrals). Diagnostic synergy is enhanced by combining such diagnostics to common viewing optics which allow exact-mapping. Soft x-ray tangential imaging has been achieved by using a two dimensional charge coupled device detector in a pinhole camera. Finally, a fast IR camera monitors the power deposition on the first wall and divertor plates, important in quantifying power losses (e.g., ELMs, disruptions), and complemented by visible viewing of the SOL, and linear D_α cameras. © *2004 American Institute of Physics.* [DOI: 10.1063/1.1789583]

I. INTRODUCTION

The interest in high spatial definition imaging in tokamaks is driven by a variety of needs such as the extremely short scale lengths encountered in transport barriers, both edge and internal. The increasing availability of two dimensional detector arrays, catering for a wide range of wavelengths, facilitates investigations of various physics phenomena in plasmas with greater depth and confidence than often afforded by the previous generation of one dimensional systems. In all systems the recent advances in definition, channel number, speed, short gating times, and sensitivity both to flux and photon energy has been remarkable over recent years and when accompanied by the customary reduction in price we can expect profound impacts on plasma diagnostics. Indeed, it is often worthwhile to reassess the value of some multichord systems with arrays of separate detectors, for example, given the advances in multichannel detectors. The high definition and the often visible light sensitivity allow for accurate mapping, either absolutely, say, to the plasma vessel, or by integrating normally separate detector systems. The Mega Amp Spherical Tokamak (MAST),[1] provides an ideal platform both in evaluating and in exploiting imaging systems, particularly when used in tandem providing synergy in diagnostic and plasma physics interpretation. We have explored the use of high definition imaging in many applications: to determine plasma edge evolution; to acquire Z_{eff} profiles using bremsstrahlung;[9] to monitor and to exploit diagnostically high energy neutral beams in determining beam particle deposition and impurity charge exchange recombination emission profiles; to measure edge infrared (IR) emission and divertor tile heat-deposition profiles and to obtain soft x-ray image evolution. We describe the viewing, diagnostic apparatus, and detector arrays, and illustrate the efficacy of the systems in examples from plasma core behavior, internal and edge transport barriers, and in the scrape-off layer (SOL) to divertor tile region.

II. MAST IMPACTS ON DIAGNOSTIC DEVELOPMENT

MAST is a second generation spherical tokamak (ST) providing low aspect ratio ($R/a \sim 1.3$), highly elongated

[a]Electronic mail: patrick.carolan@ukaea.org.uk

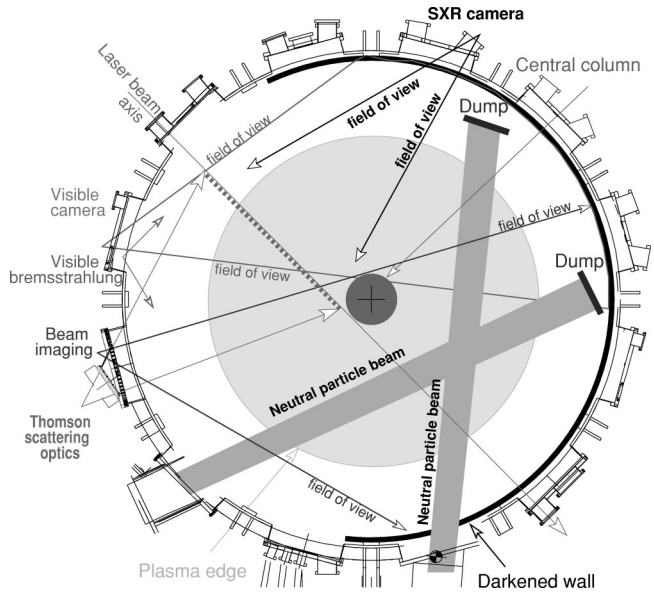

FIG. 1. (Color online) Plan view of the MAST mid-plane showing the full diameter coverage of the TS and viewing extent of the various imaging systems as well as the NBI profiles.

($\kappa > 2$) plasmas with plasma currents and minor cross sections comparable to medium sized conventional tokamaks such as DIII-D and ASDEX-U. It also has considerable additional power, e.g. from neutral beam injection (NBI) of $\sim$5 MW, giving power and injected momentum densities comparable to, or exceeding, those of the present generation of medium and large conventional tokamaks. Access to enhanced confinement regimes typical of conventional tokamaks are readily achieved. Plasma fuelling is provided by both outboard and inboard gas puffing as well as from multipellet injection. Thus, contributions can be made to general tokamak physics investigations and scaling databases, with emphasis on the effects from small aspect ratio and low magnetic fields. This complements investigations in MAST of the physics and operating regimes of interest to developing the ST concept.

MAST provides unequalled diagnostic access to all regions of interest, from core to periphery, edge to SOL, and divertor. A plan view of the mid-plane diagnostic access in MAST is shown in Fig. 1. The wide access is mainly due to the large vacuum to plasma volume ratio where the relatively remote ports allow viewing of the full quasispherical plasma, divertor regions, and beyond. The vessel wall has been sprayed with graphite in the vicinity of the mid-plane to minimize reflections; any reflections that are present (e.g., at ports) tend to be quite apparent when observed with two dimensional (2D) imaging diagnostics. Furthermore, MAST is equipped with high spatial and temporal definition internal kinetics diagnostics: Thomson scattering (TS),[2,3] (ruby laser, 300 points, single pulse; NdYAG, 19 points, 200 Hz), and charge exchange recombination (CXR) (20 chords[4] being upgraded to $>$200 chords)[6] together providing detailed profile evolution of T_e, n_e, T_i, and V_ϕ. When related to inherent plasma scale lengths, such as Larmor radius or poloidal flux, the already high definitions translate into an effective spatial resolution seldom reached by other tokamaks. These high resolutions are valuable in understanding transport barriers, where the scale length can be comparable to the ion Larmor radius. The interpretation of high-definition diagnostic systems that require profiles of the plasma kinetics can thus be fully exploited in MAST.

III. IMAGING IN DIFFERENT SPECTRAL REGIONS

The availability of high performance matrix arrays, such as charge coupled device (CCD) detectors, have revolutionized imaging diagnostics from the soft x rays to IR. The imaging diagnostics can be classified according to the technologies: (a) The visible and IR form a natural grouping

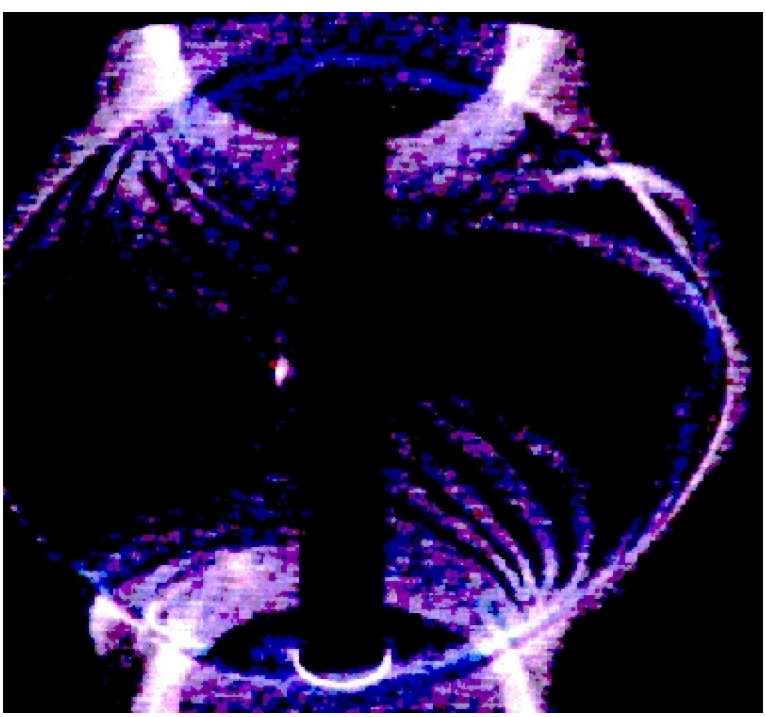

FIG. 2. High-speed video image of the MAST plasma obtained at the start of an ELM, showing evidence of a filamentary structure. In order to eliminate the background plasma light, the preceding frame has been subtracted.

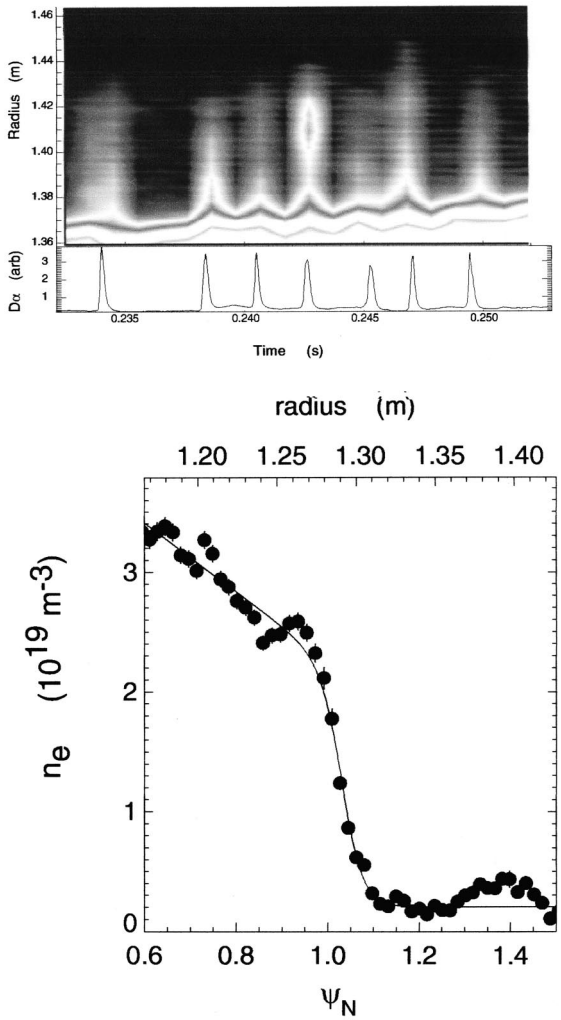

FIG. 3. When TS fires within 20 μs of an ELM a feature is sometimes (20%) observed in the n_e (and T_e) profiles well outside the LCFS. Similarly, a detached feature is observed by the linear D_α camera tangentially imaging the plasma periphery in the mid-plane.

because of the high transmittance in materials, allowing the use of lenses, fibres, etc. and operation in air. Three means of image spectral analyses are considered: (i) wide bandwidth; (ii) discrete, single and multiple, narrow bandwidths; and (iii) range of central wavelength variation along an image much in excess of bandwidth from any one region. Examples are given for each in the visible but for IR only in (i), although experiences from the visible can be transferred to the IR. Operating in the near ultraviolet (UV) to near-infrared spectral regions also avoids the complicating contribution from the recombination continuum. (b) Soft x rays generally use nonrefracting imaging, especially pinholes for wide fields of view. Spectral imaging can be achieved by various means, e.g., absorption foils, multilayered mirrors, and crystals. Another method involves pulse height analysis, (PHA),[7] allowing photon energy distributions to be determined in individual elements of a 2D detector array. Here we discuss pinhole imaging.

A. Visible and IR: broadband

1. Visible: broadband

Unfiltered, visible imaging of the plasma provides one of the principle operational tools in MAST and has made a significant contribution to the understanding of fast events such as plasma startup, ELMs and disruptions in MAST. Despite the lack of spectral resolution, high spatial and temporal resolution cameras in MAST can provide very useful data, not least because wide field-of-views encompassing both plasma poloidal cross sections are afforded by the ST and vessel geometry. At their simplest these images, which are typically dominated by Balmer D_α and CII/III emission from the edge plasma, provide a rapid postshot feedback on plasma performance, providing operational information on plasma shape, plasma conditions, global magnetohydrodynamics, gas puff operation, and unwanted interactions with in-vessel components. More detailed analysis of the images, particularly at higher frame rates, has aided understanding of transient events. Several fast video cameras are available on MAST. The highest definition one is a Phantom V4.0 from Vision Research, incorporating a color complementary metal–oxide–semiconductor chip with 512×512 pixels. This is generally run at 1 kHz giving a total recorded time of 1 s with the standard memory of 256 MB. The camera delivers a 100 000:1 blooming ratio with no pixel-to-pixel spill over and has a sensitivity equivalent to 800 ASA, allowing short integration times for transient events. Unique evidence is provided in MAST for the filamentary structure of ELMs using full plasma viewing with a short (20 μs) exposure time. Provided the plasma rotation is sufficiently slow so that the features are not blurred, clear filaments are observed as shown in Fig. 2. In this case, an exposure taken just before the ELM is subtracted from the exposure capturing the ELM, to enhance its visibility.[5] When the TS systems fire during the camera's 20 μs exposure time, in about 20% of instances significant electron densities are observed localized to a region significantly beyond the last closed flux surface, as shown in Fig. 3. Other supporting evidence shown in the figure for the filamentary nature of an ELM is obtained from a linear D_α camera viewing the plasma edge in the mid-plane; however, a 1 D diagnostic on its own would be unable to identify the complex geometric structure of an ELM. The open geometry of MAST where the plasma boundary is distant from the vessel wall allows such structures to be observed with relative ease.[8]

2. IR: broadband

A new generation of fast, IR imaging systems have become available over the last few years which are ideally suited to the open views of first wall and divertor plasma facing components in MAST. Typically these systems are used to obtain the component surface temperature, assuming blackbody IR emission at some given surface emissivity. Subsequent analysis of the temporal evolution of surface temperature using an inverse heat transfer code allows the surface power density to be derived. MAST is equipped with an IR camera operating in the 3–5 μm wavelength range, allowing the use of sapphire windows which are also trans-

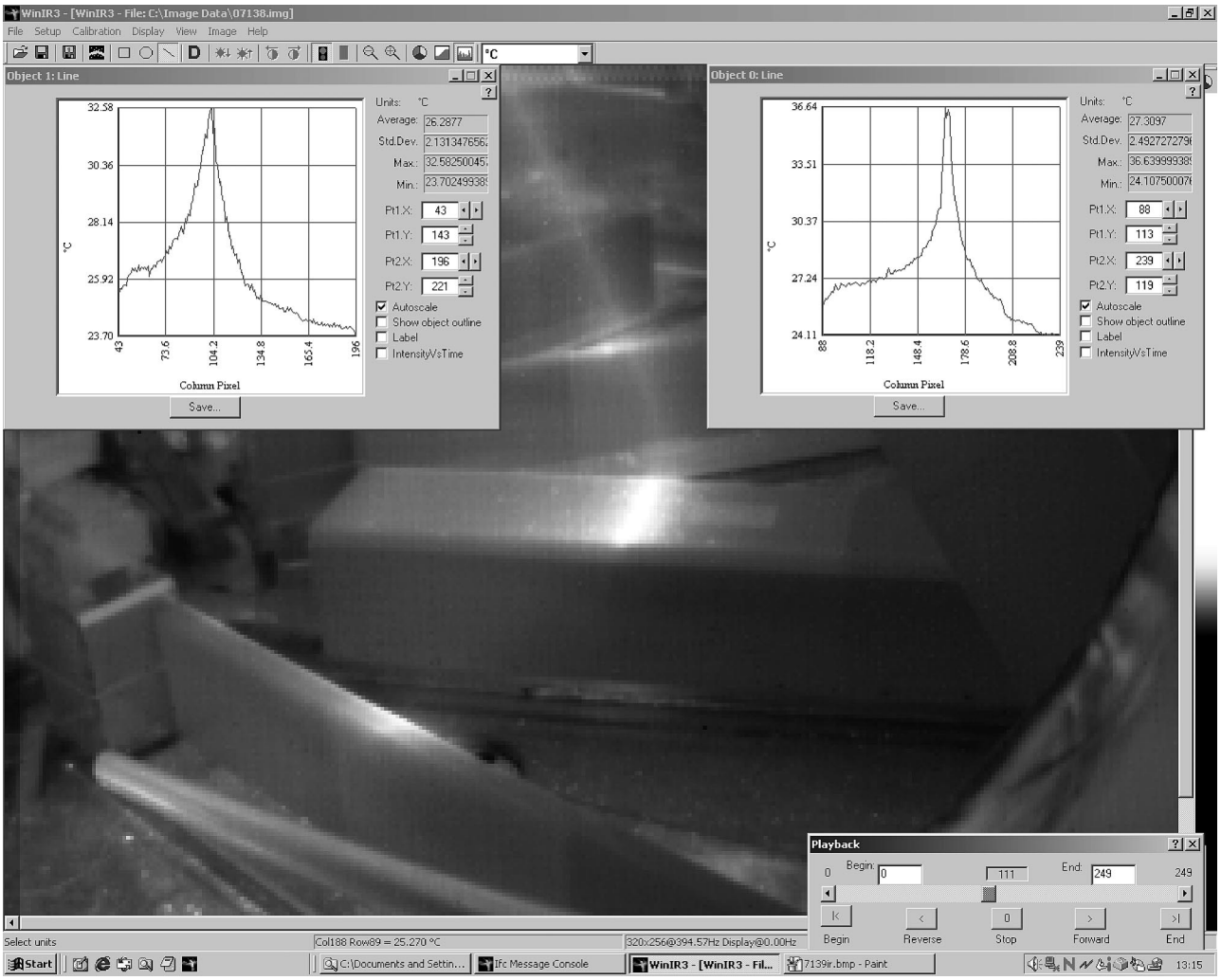

FIG. 4. IR image in the divertor region showing localized heating of graphite tiles. The graphs, top left and right, show the temperature distributions of the inner and outer strike points, respectively.

parent in the visible and near UV. The camera has a 320 $\times$256 pixel, cooled indium antimonide detector array with a full frame rate of 315 frances per second (fps) and up to 10 416 fps with reduced image format. The total system noise less is less than 20 mK with 14 bit acquisition allowing frame integration times as short as 5 μs. The camera can be fitted with a range of IR lenses, including a wide angle lens which allows over 60% of all plasma facing surfaces to be imaged. With a typical 13 mm focal length lens fitted, the spatial resolution is better than 5 mm at 2 m from the detector.

IR imaging in MAST has been used to obtain surface power densities in both steady-state and transient conditions. In steady state the analyzed IR data, which include all heat flux channels (electron, ion, and radiation), complements, and in some ways is superior to that available from embedded Langmuir probes, which are only sensitive to the electron channel. IR data obtained at high frame rates, up to 10 kHz, has been used to explore rapid changes to power deposition profiles and deposited energy during transient events, such as plasma disruptions and ELMs. An example is shown in Fig. 4 of the heat deposition in the divertor region, clearly showing different temperature profiles at the strike points. They are used in determining the heat fluxes and in estimating the contributions in the various loss channels, aided by results from the Langmuir probes.

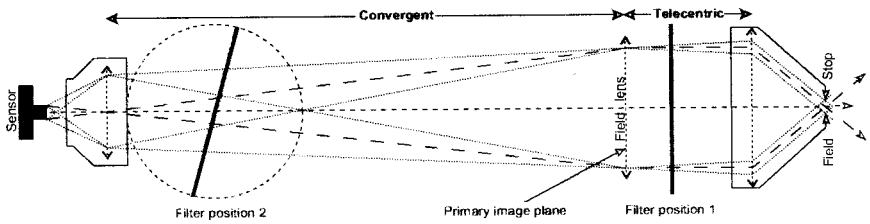

FIG. 5. Schematic of narrow band imaging optics that accommodates a wide field-of-view (note that only one of the two shown filters will be present).

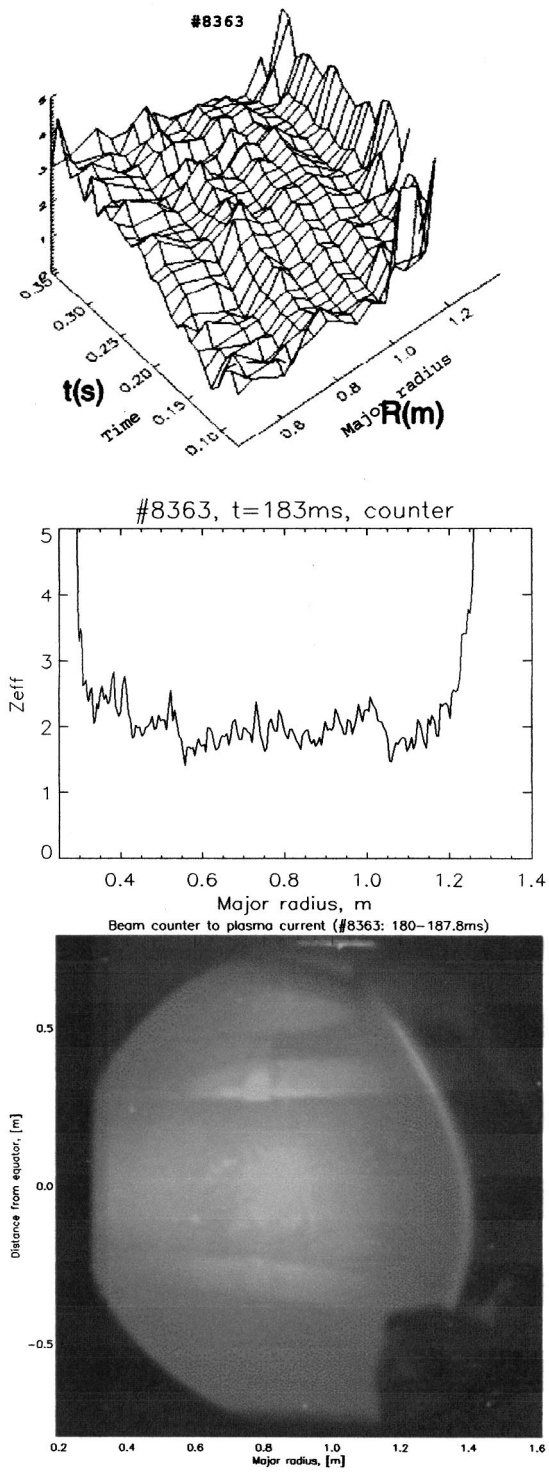

FIG. 6. Results from bremsstrahlung monitoring, showing from bottom, brightness image (single frame of 128×128 pixels, 10 ms), detailed Z_{eff} profile obtained after Abel inversion and interpreted using the 300 ruby laser TS, and, top, Z_{eff} profile evolution obtained using the 19 point, 200 Hz, NdYAG TS system.

B. Visible: wavelength filtered

In tokamaks the spectral resolution required is generally $\sim$1 nm, whether monitoring the intensity of individual spectral lines or in the sparse regions free of lines for continuum measurements. When using an interference filter (IF) this means that the light acceptance angle is only a few degrees

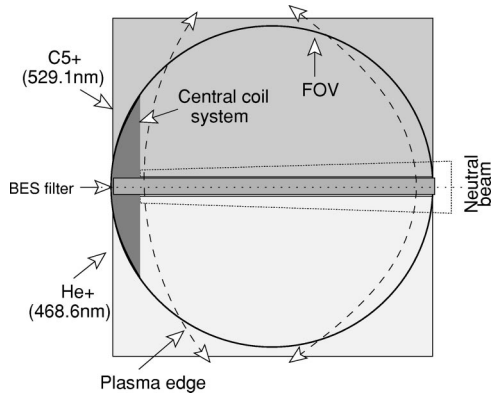

FIG. 7. Incorporation of three edge-to-edge joined filters, dividing the image of the neutral beam in the telecentric optical region (cf. Fig. 5). The central narrow and the adjacent filters select 659.5 nm (BE D_α), 468.6 nm (He^+, $n=3-4$), and 529.1 nm (C^{5+}, $n=7-8$).

whereas the field-of-view presented by the plasma imaging optics may be several tens of degrees. Both features can be accommodated without loss of *etendue* as illustrated in Fig. 5 which is the generic design of the various systems used on MAST. The aperture at the front focal plane of the plasma viewing lens, while allowing the capture of a wide field-of-view, restricts the light exiting the lens to narrow angular cones whose chief rays are parallel to the optic axis. This provides ideal illumination of an IF without loss of system etendue. The "telecentric" image produced will be largely unaffected by the IF in terms of image quality. (Achieving a compact and versatile design is discussed in detail in Ref. 9.) An example for such a system on MAST is shown in Fig. 5 (total length is $\sim$0.5 m). The CCD camera principal specifications are: total sensitive area 12.3 mm$\times$12.3 mm, 1024 $\times$1024 pixels (12 μm square), frame rate 128 Hz with maximum binning (8×8, yielding 128×128 superpixels); and frame transfer time 1 ms.

1. Full plasma viewing

Visible radiation principally comes from the edge of tokamak plasmas, in the form of spectral line emission. However, there are various sources of visible light that emit throughout the plasma volume that can be spectrally isolated by placing an IF in the telecentric region of the optics shown in Fig. 5. For bremsstrahlung, the wavelength and bandwidth are chosen to match a line free region (see Ref. 9). The continuum spectrum, $S(\omega)$, is described by

$$S(\omega) \propto \frac{n_e^2 Z_{\mathrm{eff}} \overline{g_{\mathrm{ff}}}}{T_e^{1/2}} \exp\left(-\frac{\hbar\omega}{kT_e}\right)$$

where $\overline{g_{\mathrm{ff}}}$ is the Gaunt factor. The effective charge Z_{eff} is given by $Z_{\mathrm{eff}}=\Sigma_k\,(n_k Z_k^2)/n_e$, where n_k is the density of the ion charge state Z_k.[11]

Illustrative results of Z_{eff} interpreted bremsstrahlung results are shown in Fig. 6. These results are important in calculating the plasma total resistance, and crucial when investigating enhanced resistance from neoclassical effects where MAST is particularly suited[12] because of its small aspect ratio.

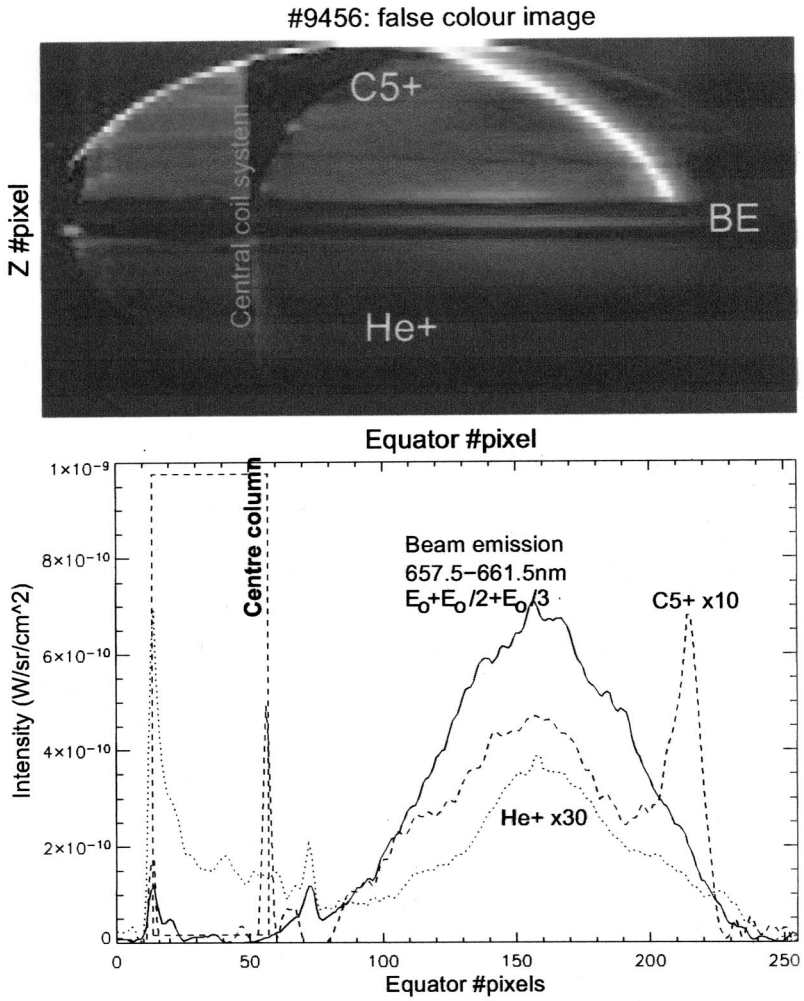

FIG. 8. (Color online) Intensity profiles of emission along the neutral beam from the Doppler shifted D_α of the fast neutrals, CXR radiation from C^{5+}, and He^+, respectively.

2. Multiwavelength plasma viewing

The use of NBI provides extensive visible emission from the edge to the plasma center: e.g., line radiation from the beam neutrals and from CXR Rydberg transitions from, originally, fully ionized impurities, generally low to medium *Z*. There are many ways in which an image may be viewed by several IFs simultaneously, (cf. Ref. 10), providing multiwavelength analysis. This is best accomplished in the telecentric region shown in Fig. 5. Here we take a simple example, shown in Fig. 7, of three IFs, joined edge-to-edge, in the primary image plane. The central IF views Doppler-shifted D_α beam emission (BE) from fast beam neutrals but excludes the unshifted emission at 656.1 nm; the other filters view the spectral lines at 468.6 and 529.1 nm, from He^+, $n=3-4$ and C^{5+}, $n=7-8$, respectively. Results can be seen in Fig. 8 where the brightness images are on the left while the distributions from the central and edge portions of the beam image are on the right. Using beam and atomic physics modeling the absolute beam neutral density may be obtained and the resulting contribution to the observed CXR impurity emission.

However, the CXR of plasma fuel ions with beam neutrals can also contribute, especially at excited states, as well as the background neutrals. To measure these an IF centered about the unshifted D_α wavelength (and excluding the Doppler-shifted BE) has also been used.[10]

3. Narrow bandpass filtering of images with spatially varying wavelengths

High energy hydrogenic neutral beams, from positive ion sources, generally have a series of discrete energies, (primarily E_0, $E_0/2$, and $E_0/3$). It can be important to monitor at least one or two of these separately in assessing performance and the energy, particle, and momentum deposition in the plasma. Assessing the behavior of the distinct fast neutrals energies in a neutral beam presents an interesting problem in distinguishing between the various components. The D_α emission from beam neutrals will have a wide range of Doppler shifts when viewed along separate lines-of-sight within a large field-of-view angle. If we are to discriminate a particular energy component from others in the beam, a relatively narrow bandpass filter is required that adjusts its central bandpass wavelength in tune with the varying Doppler shift with viewing angle. With a little care this can be accomplished[10] by providing a suitable range of chief-ray angles in the convergent region of the optics where a tilted IF provides a suitably varying central wavelength. This is possible because of the dependence of transmitted wavelength with illumination angle, i.e., $\lambda(\theta)/\lambda(0)=\{1-(1/n^2)\sin^2\theta\}^{1/2}$, where $\lambda(\theta)$ is the transmitted central wavelength for an incident angle θ, and n is the IF effective refractive index. An example of such a match of bandpass central wavelength with a range of Doppler shifts from a neutral beam on MAST

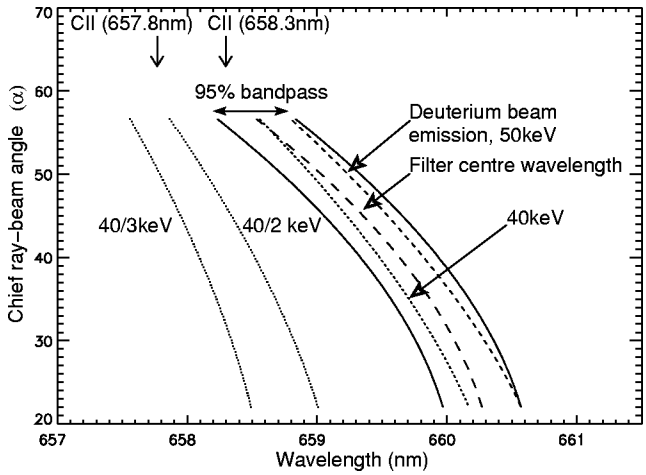

FIG. 9. Plots of the Doppler shifts from three energy components in the neutral beam (45 kV) are compared with the shifting bandpass of the IF for a range of illumination angles (α) corresponding to viewing angles of the beam.

is shown in Fig. 9. An example of the measured profile evolution of D_α emission along the beam axis from the beam primary energy component E_0 is shown in Fig. 10.

C. Soft x rays

Preliminary experiments have been conducted on MAST to assess the possibilities of soft x-ray imaging using a CCD array. The advantages of CCDs include the large number of pixels and availability of commercial camera systems. As an initial step we are availed of the same CCD camera model used for the visible imaging but stripped off the chip's protective window in air. The camera views the minor cross section in the mid-plane and is placed ~12 mm behind a 100 μm diam pinhole. The main attenuations then arise from the polysilicon electrode layer on the CCD (front illuminated chip) and the beryllium foil providing the vacuum–atmosphere interface for the pinhole viewing. Placing the

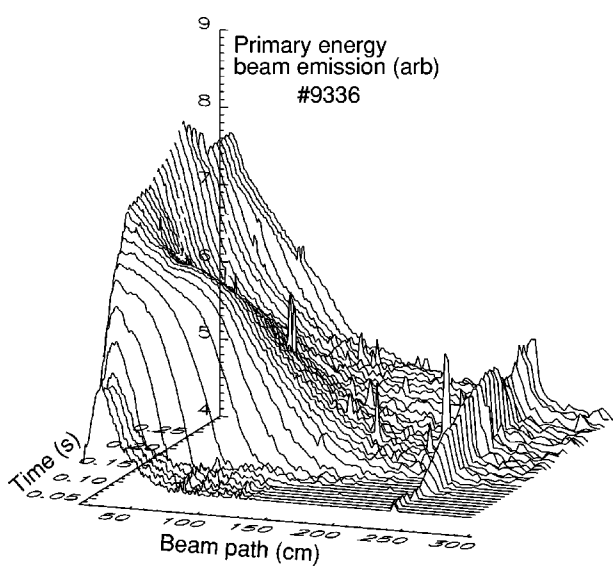

FIG. 10. Evolution of D_α emission along the axis of a neutral beam injected into a MAST plasma. Emission from the primary energy component is spectrally isolated from contributions from the other components.

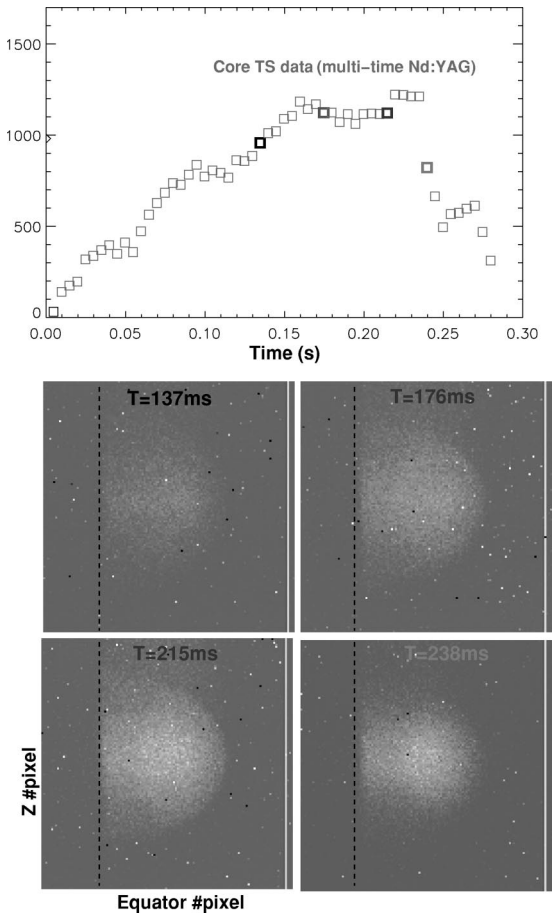

FIG. 11. (Color online) Soft x-ray image frames of a MAST plasma (No. 9575), viewed tangentially, compared with the T_e evolution, shown above. The integration time is 5.65 ms and full frame sweep time is 1.024 ms.

CCD chip close to the pinhole, required for full plasma viewing, gives acceptable attenuation in air compared with those from the beryllium foil (~10 μm) and the CCD front silicon layer ~4 μm. The Si attenuation far exceeds the Be foil ($\gtrsim$2 orders of magnitude). Thus, only photons in excess of 4 keV energy are usefully recorded. The spectrum-integrated soft x-ray brightness originating from the plasma is thus reduced by 3–4 orders of magnitude on reaching the sensitive depletion layer for typical MAST T_e of 1 keV, greatly reducing the effective time resolution compared with back-illuminated CCDs but easing the conditions to record photons separately on individual pixels. The photon fluxes and energies typically emitted from MAST plasmas mean that, depending on CCD framing time, the camera can collect total soft x-ray flux imaging or can capture photon-event images providing spectral information through PHA of individual pixel signals, when there are sparse counts per frame to reduce pulse-pileup effects. The relatively poor sensitivity and the fact that the image data consist of chord-integrated spectral brightnesses make for difficult unfolding and statistical analyses, not addressed here. However, some preliminary results are shown in Fig. 11, illustrating total flux images of a MAST plasma as the T_e evolves during a shot.

ACKNOWLEDGMENTS

The authors are grateful to the MAST Physics, Engineering, Data Acquisition and Neutral Beam teams, and to Oak

Ridge National Laboratory for loaning neutral beam equipment on MAST. Special thanks also go to B. Lloyd, A. W. Morris, and A. Sykes for many discussions and assistance and to R. Gaffka for help in the design of the soft x-ray camera at short notice. This work was funded jointly by the United Kingdom Engineering and Physical Sciences Research Council and by EURATOM.

[1] A. Sykes *et al.*, Phys. Plasmas **8**, 2101 (2001).
[2] M. J. Walsh, E. R. Arends, P. G. Carolan, M. R. Dunstan, M. J. Forrest, S. K. Nielsen, and R. O'Gorman, Rev. Sci. Instrum. **74**, 1663 (2003).
[3] M. J. Walsh *et al.*, Rev. Sci. Instrum., these proceedings.
[4] P. G. Carolan *et al.*, Rev. Sci. Instrum. **68**, 1015 (1997).
[5] A. Kirk *et al.*, 30th EPS. Conference on Controlled Fusion and Plasma Physics, St. Petersburg, Russia, 2003, 27A, p.3.201.
[6] N. J. Conway, M. J. Walsh, P. G. Carolan, C. A. Bunting, and M. R. Dunstan, Rev. Sci. Instrum. (submitted).
[7] Y. Liang, K. Ida, S. Kado, T. Minami, S. Okamura, I. Nomura, K. Y. Watanabe, and H. Yamada, Rev. Sci. Instrum. **72**, 717 (2001).
[8] A. R. Field *et al.*, 30th EPS Conference on Controlled Fusion and Plasma Physics, St. Petersburg, Russia, 2003, Vol. 27A, p.3.93.
[9] A. Patel, P. G. Carolan, N. J. Conway, and R. J. Akers, Rev. Sci. Instrum. (submitted).
[10] A. Patel *et al.*, Rev. Sci. Instrum., these proceedings.
[11] Dalstar camera model:1M30P, see <http://www.dalsa.com> and <http://www.firstsightvision.co.uk/>
[12] R. J. Akers *et al.* (unpublished).